Journal of Ceramic Processing Research. Vol. 25, No. 5, pp. 862~870 (2024)
(Received 11 July 2024, Received in revised form 23 July 2024, Accepted 11 September 2024)
https://doi.org/10.36410/jcpr.2024.25.5.862

J O U R N A L O F
Ceramic Processing Research

Study on properties of slag - heavy calcium powder - cement composite cementitious materials

Youshuai Zhao[a], Xuetao Yue[a,*], Yuhan Tang[a], Xuelei An[b] and Xiaopeng Shang[c]
[a]*School of Material Science and Engineering, Shandong Jianzhu University, Jinan 250101, China*
[b]*Shandong Survey and Design Institute of Water Conservancy Co., Ltd, Jinan 250013, China*
[c]*Shandong Urban Construction Vocational College, Jinan 250103, China*

The effects of heavy calcium powder and slag together as auxiliary cementitious materials on the compressive strength of cementitious sand and the synergistic effects were investigated. The hydration products, microscopic morphology and pore size distribution of cementitious materials were studied by X-ray diffraction (XRD), scanning electron microscopy (SEM), heat of hydration method, nuclear magnetic resonance (NMR) technique and mercury intrusion porosity (MIP). The results show that the strength of cement mortar being mixed with heavy calcium powder and slag is higher than that of single slag, and higher than that of pure cement mortar in the later stage. Heavy calcium powder particles become the core of cement hydration product growth, and promote cement hydration, so that the hydration products are tightly bound; heavy calcium powder later has hydration, and reacts with the aluminum phase in slag to generate calcium monocarboaluminate hydrate ($Ca_4Al_2O_6{\cdot}CO_3{\cdot}11H_2O$), which improves the pore size distribution of cement paste and refines the pore size. This is the main reason that heavy calcium powder and slag as an auxiliary cementitious material improve the strength of cement mortar.

Keywords: Heavy calcium powder, Supplementary cementitious material, Porosity, Microstructure.

Introduction

Cement is one of the indispensable materials for the construction, transportation, and water conservancy industries, and a large amount of carbon dioxide is generated during the production process. It is estimated that the greenhouse gases emitted from the production of cement worldwide account for about 7% of the total greenhouse gas emissions of the earth's atmosphere [1], and the energy consumed by cement production accounts for about 15% of the total global industrial demand [2]. The total amount of cement produced globally in 2023 is 4.072 billion tons, and the carbon dioxide produced from cement production is approximately 1.2 billion tons. In order to reduce greenhouse gases emissions during the production of silicate clinker, many measures have been proposed by the industry: improving the energy efficiency of kilns and precalciner furnaces, improving grinding efficiency, fuel substitution, raw material substitution, and the use of auxiliary cementitious materials to replace clinker, among other technological solutions [3-6]. Replacing cement with calcined clay limestone is one of the most effective technologies, which can reduce clinker demand by about 27%, followed by reducing the amount of cement used in concrete, thereby reducing carbon dioxide emissions by 10% [7-9].

It has been shown [10] that mixing limestone powder from 0% (mass fraction, the same below) to 20% will optimize the chlorine penetration resistance of low-strength concrete, but will weaken its freeze-thaw resistance.Golaszewski, J et al. [11] found that concretes with limestone powder did not significantly differ in frost resistance from reference concretes. When 10% limestone powder and 10% fly ash are added, the compressive mechanical properties of concrete are better than ordinary concrete, and the freeze-thaw resistance is similar [12-16]. Heavy calcium powder, mainly composed of calcium carbonate, is a white powder made by grinding limestone. As an industrial by-product of crushing limestone and producing mechanism sand in quarries, heavy calcium powder is not only inexpensive and stable in composition, but also does not require calcination, has good grindability, and is easy to transport. As an auxiliary cementitious material, it partially replaces cement and effectively reduces carbon emissions in cement production. Slag is industrial waste residue, while heavy calcium powder is an industrial by-product of crushing limestone and producing mechanism sand in quarries. The prices of slag and heavy calcium powder per ton are 165-175 CNY and 100-200 CNY respectively, while the price of cement is 400-500 CNY. The prices of slag and heavy calcium powder are 1/3 and 1/4 of cement, and their costs are much

*Corresponding author:
Tel : +86 1359035658
Fax: +86 053186367285
E-mail: yuexuetao@sdjzu.edu.cn

lower than cement. Adding them will reduce the overall material preparation cost. In the production of cement and concrete, the use of heavy calcium powder to partially replace cement has significant economic and social benefits. In addition, aluminum silicate-based supplementary cementitious materials and limestone co-replace cement can improve the reactivity of limestone to a certain extent [17-19].

Based on the above background, this paper uses crude heavy calcium powder together with slag to replace cement for experiments to study the amount of heavy calcium powder and the synergistic effect with slag and other factors, to qualitatively analyze the effect of heavy calcium powder on the hydration and hardening mechanical properties and microstructure of cement matrix, and to provide a theoretical basis for the use of heavy calcium powder as an auxiliary cementitious material.

Materials and Methods

Materials

Cement: 42.5 Ordinary Portland cement produced by Shangheshanshui Cement Co., Ltd. with specific surface area of 7297.763 cm^2/cm^3, and chemical compositions are shown in Table 1.

Slag: S95 grade slag produced by Hongsheng Mine Product Processing Factory of Lingshou County, with specific surface area of 9227.656 cm^2/cm^3, and chemical compositions are shown in Table 2.

Heavy calcium powder: 325 mesh heavy calcium carbonate produced by Henan Platinum Casting Materials Co., Ltd, and chemical compositions are shown in Table 3.

Specimen preparation

The raw materials are weighed and mixed evenly according to the designed mixing proportion, and then the water with the designed dosage is weighed and poured into the cement mortar mixing pot and then stir evenly. The slurry is injected into the 40 mm×40 mm×160 mm triplex cementitious sand test mold, and placed in the constant temperature and humidity curing box, under the condition of setting temperature (20±2) °C and relative humidity (98±2)%, the mold is demolded after 1 day, and then continues to maintain under the condition until the specified age.

In order to study the influence of the addition of heavy calcium powder on the hydration of mineral powder and cement composite cementitious materials, the water-binder ratio was kept at 0.5. Cement was set as all cementitious materials as the control group. The total

Table 1. Chemical compositions of cement.

Composition	CaO	SiO_2	Al_2O_3	MgO	Fe_2O_3	K_2O	Na_2O
Quality fractions(%)	62.48	17.58	4.21	1.67	3.21	0.58	0.23

Table 2. Chemical compositions of slag.

Composition	CaO	SiO_2	Al_2O_3	MgO	Fe_2O_3	TiO_2	K_2O	Na_2O
Quality fractions(%)	40.24	27.11	14.31	7.30	0.45	1.45	0.46	0.60

Table 3. Chemical compositions of heavy calcium powder.

Composition	$CaCO_3$	SiO_2	Al_2O_3	MgO	Fe_2O_3
Quality fractions(%)	98.56	0.20	0.27	0.16	0.02

Table 4. Cement mortar mix ratio of slag- heavy calcium powder -cement composite cementitious materials.

No.	cement/g	Calcium carbonate/g	slag/g	water/g	sand/g	water-binder ratio
H_0S_0	450	0	0	225	1350	0.5
H_0S_{100}	225	0	225.00	225	1350	0.5
H_5S_{95}	225	11.25	213.75	225	1350	0.5
$H_{10}S_{90}$	225	22.50	202.5	225	1350	0.5
$H_{15}S_{85}$	225	33.75	191.25	225	1350	0.5
$H_{20}S_{80}$	225	45.00	185	225	1350	0.5
$H_{25}S_{75}$	225	56.25	168.75	225	1350	0.5

Note: H means heavy calcium powder, S means slag.

content of slag and heavy calcium powder was fixed as one-half of the cementitious material, and the content of heavy calcium powder was changed. The test mix ratio is shown in Table 4.

Testing methods

Compressive strength

According to the Chinese standard GB/T 17671-2021, the compressive strength test was carried out by WDW-100A universal testing machine, with a compressive loading rate of 2400 N/s±200 N/s. The compressive strength of the specimen was obtained from the average of a group of 6 samples, and the test error was required to be less than 10%.

XRD

The hydration products of specimens were determined by XRD. The target material of the X-ray tube was Cu. It scanned from 5° to 90°. It scanning step size and a continuous scanning mode.

SEM

Observation of the micro-morphology of the samples' surfaces with a thermal field emission scanning electron microscope (SUPRA™55).

Hydration heat

The exothermic process of cement hydration was monitored with a TAM Air eight-channel isothermal calorimeter. Before the test, the same mass of the specimen was weighed and placed into the test vials, which were then sealed with a lid and placed into the calorimeter, and the exothermic change in the cement for the first 3 d of hydration was recorded. This experiment was carried out at a constant temperature of 20 °C, and the interval of data collection was 30s.

MIP

The porosity of the samples was tested by McMurray Tick (Shanghai) Co., Ltd. The contact angle was 130°, and the applied pressure ranged from 0.10 to 61000.00 psia.

NMR

The Lime-MRI-D2 low-field NMR system from Beijing Limecho Technology Co., Ltd was used to obtain T_2 spectra. The magnetic field strength of this equipment is 0.3±0.05 T, and the operating temperature is 22~28 °C. The specimen is a cylinder 40 mm in diameter and 40 mm in height.

In this paper, the pores are categorized into 4 types: gel pores (I, <10 nm), transition pores (II, 10~100 nm), capillary pores (III, 100~1,000 nm), and air-pores or fissures (IV, >1,000 nm) [20].

The NMR test was performed by measuring the strength of the hydrogen ion signal in the pore water of the specimen and using mathematical inversion to obtain the T_2 relaxation time spectrum. The horizontal coordinate of the T_2 relaxation curve reflects the pore size of the concrete, and the size of the horizontal coordinate is proportional to the pore size; the amplitude of the signal in the longitudinal coordinate reflects the number of pores, and the larger the longitudinal coordinate is, the more pores there are. The magnitude of the longitudinal coordinate reflects the number of pores, and the larger the longitudinal coordinate is, the greater the number of pores. According to the literature [21], the T_2 relaxation time is shown in Eq. (1).

$$\frac{1}{T_2} = \frac{1}{T_2 B} + \frac{1}{T_2 D} + \frac{1}{T_2 S} \tag{1}$$

where T_{2B} is the free relaxation time, T_{2D} is the diffusion relaxation time, and T_{2S} is the surface relaxation time.

In this test, the specimen is placed in a uniform magnetic field with short echoes so that T_{2B} and T_{2D} can be neglected [22, 23], and the relationship between the relaxation time and the hole diameter is shown in Eq. (2)

$$\frac{1}{T_2} = \rho \frac{J}{r} \tag{2}$$

the lateral surface relaxation rate, 0.001 cm/s [24, 25]; J is the pore shape factor; and r is the pore diameter.

Assuming that the pore shapes are all columnar, Eq. (2) can be expressed as

$$r = 2\rho T_2 = CT_2 \tag{3}$$

Therefore, C=20 nm/ms, equation (3) can be expressed as

$$r = 20T_2 \tag{4}$$

Results and Discussion

Compressive strength

Fig. 1 shows the compressive strength of mortar with slag-heavy calcium powder-cement composite cementitious material at different ages. It can be seen from the figure, the compressive strength of each specimen is enhanced with the increasing of the

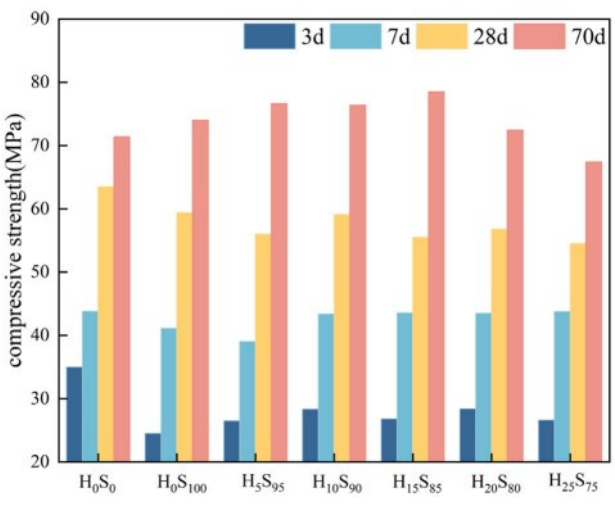

Fig. 1. Compressive strength of slag- heavy calcium powder -cement composite at different ages.

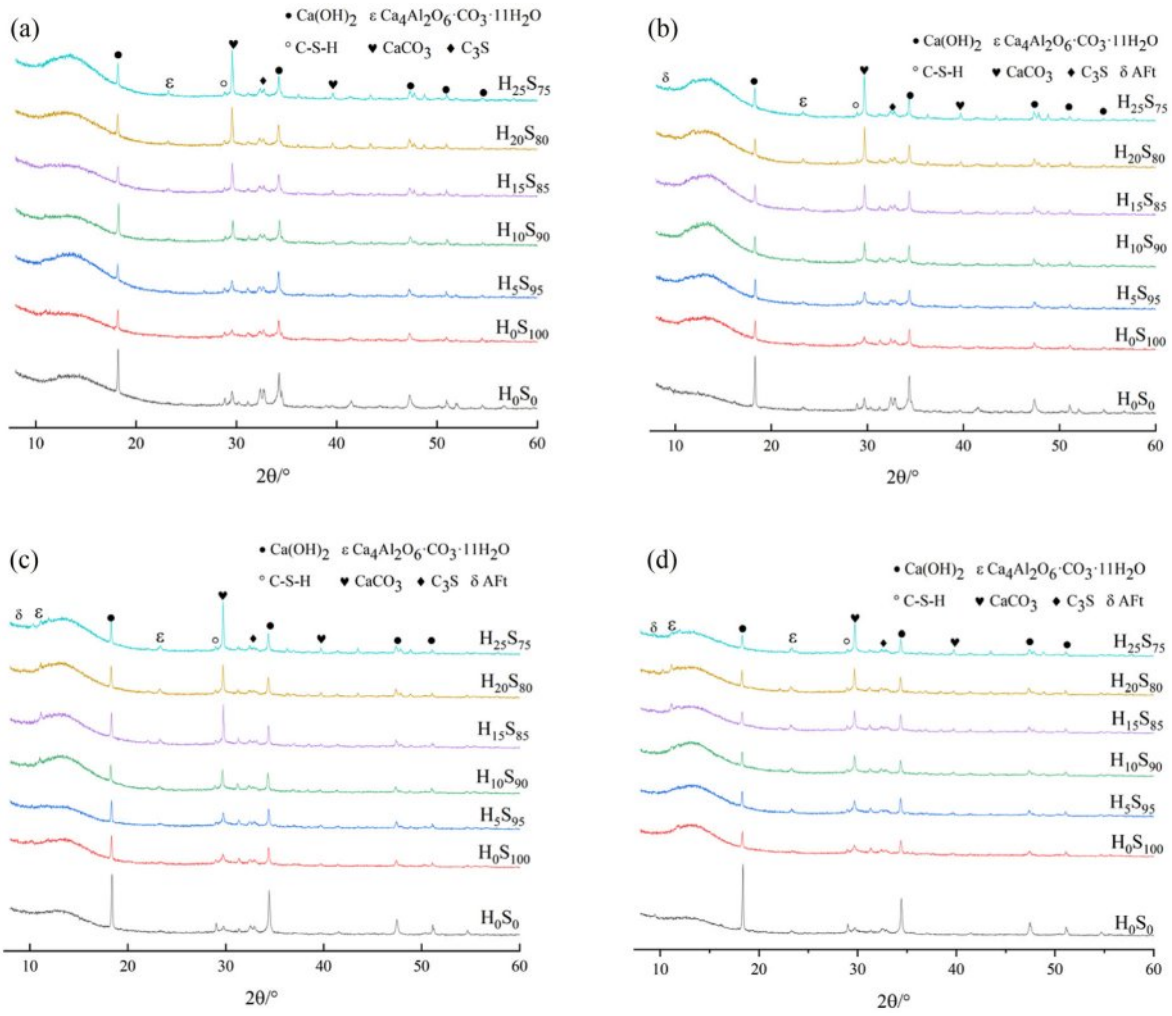

Fig. 2. XRD images of different hardened pastes at different ages: (a) 3d, (b) 7d, (c) 28d, (d) 70d.

maintenance time, of which the growth rate is the largest before 7 d, slightly slower growth range before 28 d, and the growth rate is smaller and stabilizes after 28 d. In addition, the compressive strength of single-doped slag and heavy calcium powder-slag double-doped specimens are lower than the H_0S_0 group benchmark specimens at 28 d. The reason is that the activity of slag and heavy calcium powder is lower than that of cement, and the amount of cement is reduced by 50%, by reducing the early strength of the specimen. With the extension of maintenance time, the compressive strength of double-doped specimens had a greater development, and by 70 d, the compressive strength of the double-doped specimens and single-doped slag specimens exceeded the benchmark specimens except for $H_{25}S_{75}$, and the strength of $H_{25}S_{75}$ is also close to that of the benchmark specimen. The main reason is that the activity of slag is larger than that of heavy calcium powder, and the compressive strength of the specimen increases with the increase of its reaction. Due to the low activity of heavy calcium powder, it does not participate in the hydration reaction in the early stage and mainly plays the filling effect of micro aggregate. It can be seen from the diagram that the effect is better when the content of heavy calcium powder is 10-20% of the slag content. When the content of heavy calcium powder is too much, the content of slag will be reduced, and the activity effect will be reduced, resulting in reduced strength. Overall, although the strength of the heavy calcium powder-slag double-doped specimen is slightly lower than that of the reference specimen at 28 d, the strength grade is still much higher than 42.5 MPa, and the strength of the specimen basically exceeds that of the reference specimen at the later stage of development.

XRD

It can be seen from Fig. 2 and Fig. 3(a) that H_0S_0 did not produce new hydration products with the increase of curing age, and the peak of C-S-H gel was not obvious in the early stage. With the increase of curing age, more prominent diffraction peaks were observed at 28 d and 70 d. The diffraction peak of ettringite (AFt) began to be prominent at 7 d and reached the highest at 70 d. $Ca(OH)_2$ is the main hydration product with strong

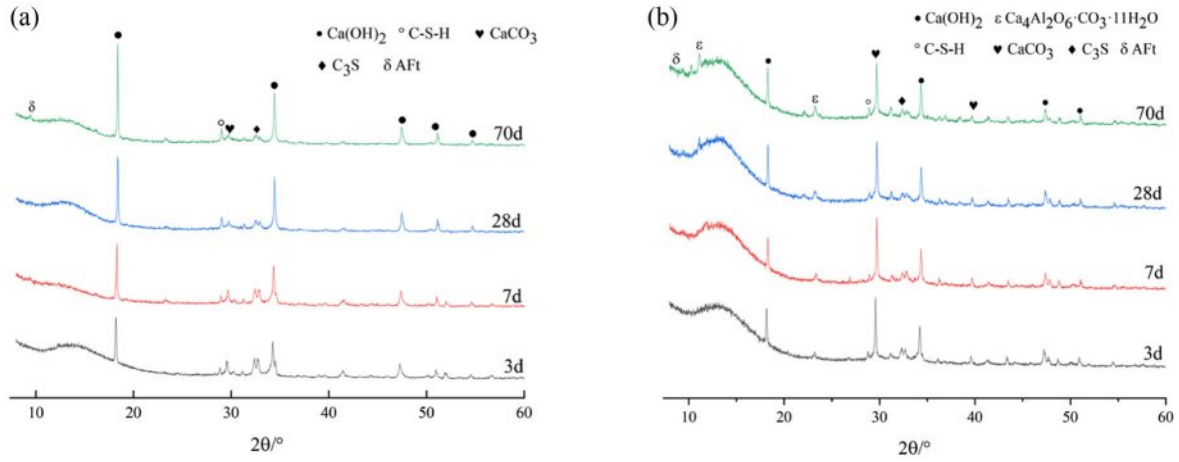

Fig. 3. XRD images of the same hardened paste at different ages: (a) H_0S_0, (b) $H_{20}S_{80}$.

diffraction peaks at all ages. The peak of C_3S gradually decreases and the hydration degree increases with the increase of age.

Fig. 2 intuitively shows that after the incorporation of slag and heavy calcium powder, the diffraction peak of $CaCO_3$ gradually increases with the increase of the content of heavy calcium powder. And the content of $Ca(OH)_2$, the main hydration product, is significantly lower than that of H_0S_0 because the content of cement clinker such as C_3S is reduced by 50%. Moreover, the content of $Ca(OH)_2$ generated by hydration of each group with slag is the highest at 28 d, and it decreases at 70 d. This is due to the secondary hydration reaction of the reactive substances such as SiO_2 in slag with $Ca(OH)_2$ [26, 27], so that $Ca(OH)_2$ is continuously consumed to generate hydrated calcium silicate, which increases the diffraction peak of the C-S-H gel and improves the late strength of the specimen. It can be seen from Fig. 2 and Fig. 3(b) that the diffraction peak of $CaCO_3$ decreases continuously with the extension of the age of maintenance, which is due to the reaction of the carbonate produced by the dissolution of heavy calcium powder with the aluminum phase in cement and slag to produce the $Ca_4Al_2O_6{\cdot}CO_3{\cdot}11H_2O$ [28-30], and the CO_3^{2-} generated in the hydration process will play a role of crystal nucleus [31, 32], promote both the hydration of cement and the development of late strength.

SEM

It can be seen from Fig. 4(a) that when H_0S_0 was hydrated to 28 d, needle-like AFt intertwined with cubic massive $Ca(OH)_2$ and granular C-S-H gel clustered together, and there was a small amount of lamellar structure around it. The overall structure was relatively dense. There were only some small pits and holes on the surface of the sample, and there was no obvious crack pattern. With the extension of hydration age, it can be seen in Fig. 4(b) that the hydration products of 70 d increase greatly and are closely intertwined with each other. Some needle-like AFt transforms into monosulfoaluminate (AFm), and the overall structure is more compact.

It can be seen from Fig. 4(c) that a large number of granular C-S-H as well as a small amount of flake AFt form a thin layer attached to the surface of heavy calcium powder particles in $H_{10}S_{90}$ specimens at the age of 28 d, and can be seen in the $H_{20}S_{80}$ specimens in Fig. 4(e) that a large amount of flake AFt and granular C-S-H gel are formed on the pit surface of heavy calcium powder particles and cement slurry matrix, and there are also a large number of C-S-H gel spread and grow around, and the structure is relatively dense. It can be seen that under the condition of heavy calcium powder particles, the hydration products will grow with heavy calcium powder particles as the core and fill the gap of the contact surface. Fig. 4(d) shows that when the hydration age reaches 70 d, the hydration products on the surface of heavy calcium powder particles have condensed a thick layer and are closely integrated with the surrounding cementitious material matrix. In Fig. 4(f), the hydration products in the pit where the heavy calcium powder particles are located are no longer piecemeal, but closely connected, and almost formed a plane. This is because the active oxide in the slag and $Ca(OH)_2$ hydrated again at the later stage of hydration, resulting in a large number of C-S-H and other hydration products intertwined, forming a relatively dense network structure, so that the heavy calcium powder particles are more closely connected to the cementitious material matrix.

Hydration heat

Fig. 5 shows the hydration exothermic rate and the cumulative hydration exothermic amount for 72 h containing different specimens. As can be seen in Fig. 5, the heat of hydration can be divided into five phases: dissolution, induction, acceleration, deceleration, and diffusion, which is consistent with the results of previous

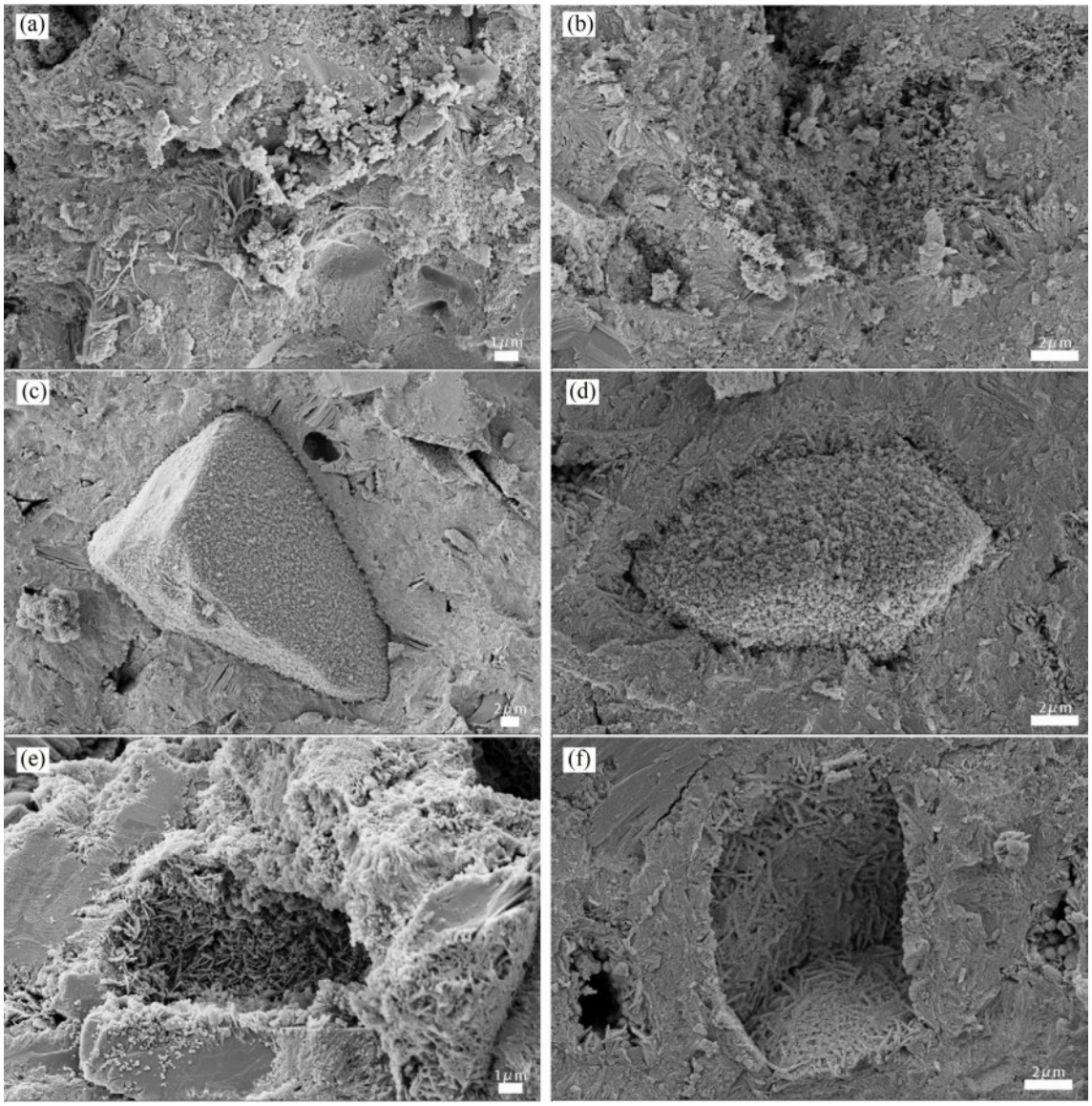

Fig. 4. Micro-morphology of different hardened pastes at different ages: (a) H_0S_0 28d, (b) H_0S_0 70d, (c) $H_{10}S_{90}$ 28d, (d) $H_{10}S_{90}$ 70d, (e) $H_{20}S_{80}$ 28d, (f) $H_{20}S_{80}$ 70d.

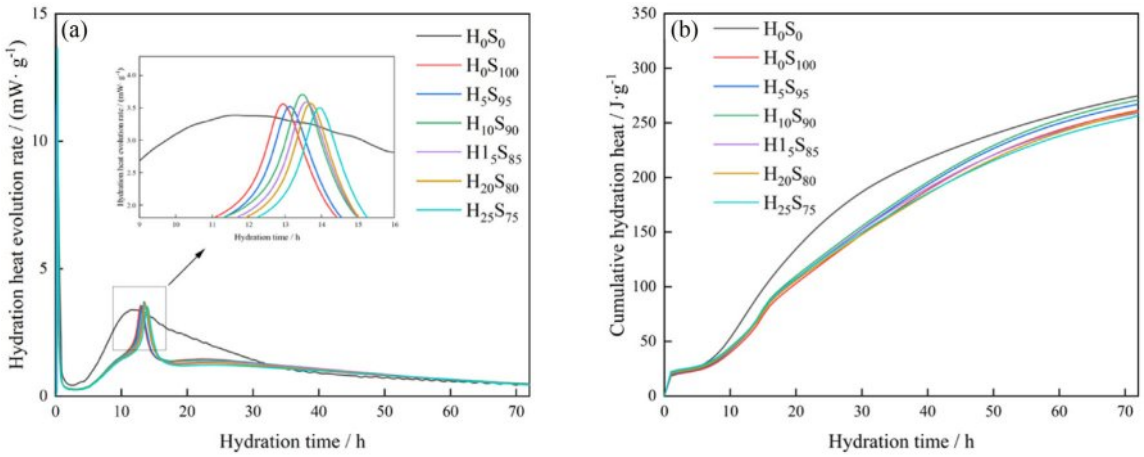

Fig. 5. Hydration heat release rate and cumulative heat release of different samples: (a) Hydration exothermic rate, (b) Cumulative hydration heat.

studies [33, 34]. As shown in Fig. 5(a), there are two peaks in each hydration heat flow curve.According to studies [35-37], the first peak is located at about 0-3 hours, which is due to the formation of AFt from C_3A and C_3S which are partially dissolved upon contact between cement and water. The second peak (about 12 hours) is caused by the accelerated consumption of C_3S and the formation of the corresponding hydration products. The exothermic peak keeps moving to the right as the content of the heavy calcium powder increases. This is due to the fact that the $CaCO_3$ acts as an inert material due to its low activity in the initial stage, while the increase in $CaCO_3$ doping reduces the C_3S content in the system, which leads to a longer time for the ions in the system to reach saturation, and thus slows down the formation of hydration products.

Fig. 5(b) shows the cumulative exothermic curve of hydration, and it can be seen that the addition of heavy calcium powder decreases the cumulative exothermic amount of the system because the addition of heavy calcium powder replaces part of the cement, resulting in a decrease in the amount of reactants and a decrease in the exothermic amount of hydration reaction.

MIP

Fig. 6 shows the pore size distribution curves for several compositions of mortar at a curing time of 28d. The pore sizes corresponding to the peaks are the most likely pore sizes, and the closer the peaks are to the left, the smaller the pore sizes. The test shows that the incorporation of slag and heavy calcium powder does not change the most probable pore size of the specimen compared to the pure cement specimen.

Fig. 7 shows the percentage of pores of mortars of several compositions at the curing time of 28d. As can be seen from Fig. 7, the percentage of gel pores of H_0S_0 pure cement-hardened mortar is the least among all groups; when slag and heavy calcium powder are mixed in, the percentage of gel pores begins to increase, but the pores and cracks also change to different degrees. 50% cement

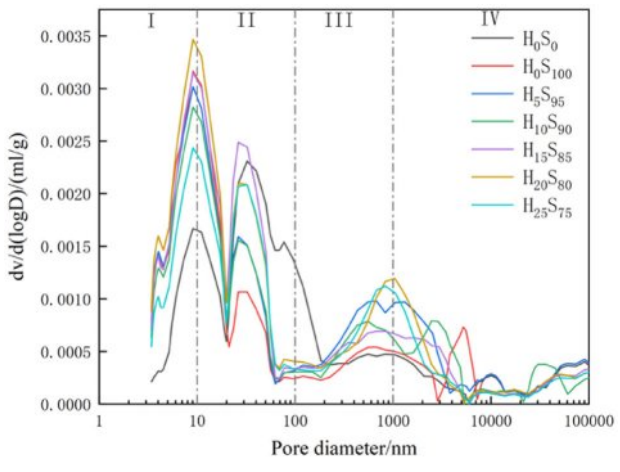

Fig. 6. Pore size distributions of mortar.

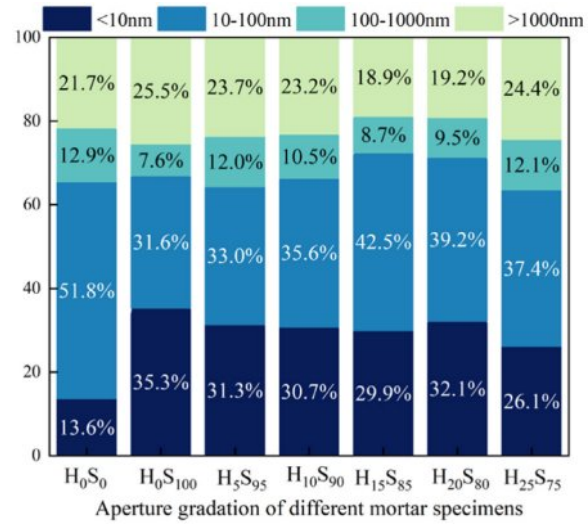

Fig. 7. Aperture gradation of mortar.

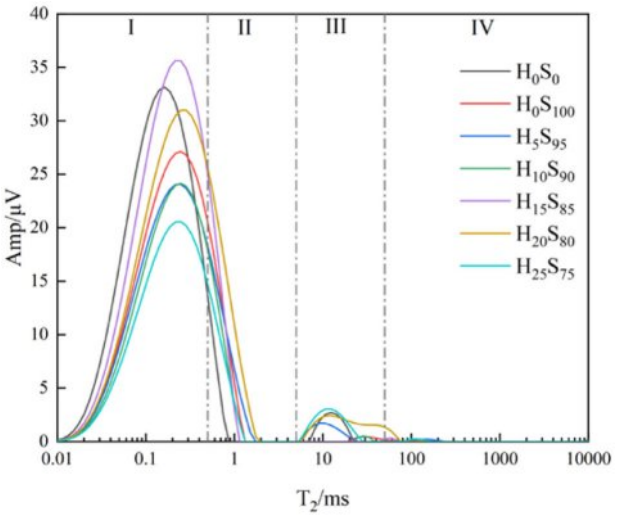

Fig. 8. T2 relaxation time spectrum of different specimens at 70d.

is replaced by slag, its percentage of gel pores is the largest, but its pores and cracks are also the most; and when part of slag is replaced by heavy calcium powder for compounding, the percentage of gel pores decreased, but so did the pores and cracks. This indicates that, at 28d, the doping of slag and heavy calcium powder, carried out began to carry out the second hydration, the hydration products generated to fill in some of the large pores, thus changing the pore size. From Fig. 3 and Fig. 4, it can be seen that at this time there is still a large amount of heavy calcium powder exists, and its degree of reaction is small, so there are still some pores and cracks exist.

NMR

The NMR test was performed by measuring the strength of the hydrogen ion signal in the pore water of the specimen and using mathematical inversion to

obtain the T_2 relaxation time spectrum. The horizontal coordinate of the T_2 relaxation curve reflects the pore size of the concrete, and the size of the horizontal coordinate is proportional to the pore size; the amplitude of the signal in the longitudinal coordinate reflects the number of pores, and the larger the longitudinal coordinate is, the more pores there are.

Fig. 8 shows the T_2 relaxation time spectrum of mortars of several compositions at a curing time of 70d. Compared with Fig. 6, it can be observed that the holes of all specimens are dominated by gel holes, and basically no air holes and cracks can be observed. This indicates that with the increase of the curing time, the hydration degree of the mineral powder and the heavy calcium powder further deepened, and more hydration products were generated, which continuously filled into the macropores.

Therefore, although the average particle size of heavy calcium powder used in this experiment is larger than that of cement and slag, it still has the effect of improving the pore size, reducing the content of harmful pores, increasing the content of less harmful and harmless pores, making the pore size distribution more reasonable, and reducing the most probable pore size of the specimen, which plays a role in refining the pore size.

Conclusion

(1) The strength of cement mortar mixed with heavy calcium powder and slag is greater than that of slag alone. The strength in the early stage is comparable to that of pure cement mortar, and the later stage exceeds that of pure cement mortar. That is, heavy calcium powder and slag have synergistic effect to improve the strength of cement mortar. In this test, when the content of heavy calcium powder accounted for 5%~15% of the total amount of heavy calcium powder-slag mixed, the strength in the later stage is more improved.

(2) The heavy calcium powder has hydration effect after 28 d, and reacts with the aluminum phase in slag to form monocarbon calcium aluminate, which improves the pore size distribution of cement paste and refines the pore size. Heavy calcium powder becomes the core of cement hydration product growth, and promotes cement hydration, which makes hydration products closely integrated and reduces pore size.

References

1. M. Ali, M.S. Abdullah, and S.A. Saad, Adv. Mater. Res. 1115 (2015) 137-141.
2. V. Sousa, J.A. Bogas, S. Real, and I. Meireles, Environ. Sci. Pollut. R. 30[4] (2023) 8778-8789.
3. S.A. Miller, V.M. John, S.A. Pacca, and A. Horvath, Cem. Concr. Res. 114 (2018) 115-124.
4. M. Schneider, M. Romer, and M. Tschudin, Cem. Concr. Res. 41 (2011) 642-650.
5. Y. Rho and S.G. Kang, J. Ceram. Process. Res. 21[S1] (2020) 74-80.
6. M. Verapathran, S. Vivek, G.E. Arunkumar, and D. Dhavashankaran, J. Ceram. Process. Res. 24[01] (2023) 89-97.
7. W. Shanks, C.F. Dunant, M.P. Drewniok, R.C. Lupton, A. Serrenho, and J.M. Allwood, Resour. Conserv. Recy. 141 (2019) 441-454.
8. S. Janani, G.S. Rampradheep, P. Kulanthaivel, and P.C. Murugan, J. Ceram. Process. Res. 23[6] (2022) 884-891.
9. S. Shanmughan, S.K. Kaliyannan, S. Marasamy, and P. Thiyagarajan, J. Ceram. Process. Res. 24[1] (2023) 111-119.
10. S. Adu-Amankwah, M. Zajzc, J. Skocek, J. Nemecek, M. Ben Haha, and L. Black, Constr. Build. Mater. 307 (2021) 125087.
11. J. Golaszewski, M. Golaszewska, and G. Cygan, Buildings 12[11] (2022) 2003.
12. B.X. Li, J.L. Wang, and M.K. Zhou, Constr. Build. Mater. 23[8] (2009) 2846-2850.
13. W.Y. Zhang, S. Na, J. Kim, H. Choi, and Y. Hama, Mater. Struct. 50 (2017) 171.
14. C.W. Hong, J.I. Lee, and J.H. Ryu, J. Ceram. Process. Res. 17[7] (2016) 768-772.
15. J. Wang, K. Xu, and Z. Li, J. Ceram. Process. Res. 23[1] (2022) 79-85.
16. L. Shen, Q. Li, W. Ge, and S. Xu, Constr. Build. Mater. 239 (2020) 117882.
17. Y. Dhandapani, M. Santhanam, G. Kaladharan, and S. Ramanathan, Cem. Concr. Res. 143 (2021) 106396.
18. D.J. Moon, Y.B. Kim, and J.S. Ryou, J. Ceram. Process. Res. 9[3] (2008) 278-281.
19. Y. Kim, B.S. Chun, and T.H. Park, J. Ceram. Process. Res. 12[2] (2011) 202-206.
20. X.H. Zeng, X.L. Lan, H.S. Zhu, G.C. Long, and Y.J. Xie, Cem. Concr. Compos. 122[7] (2021) 104139.
21. H.H. Tian, C.F. Wei, H.Z. Wei, and J.Z. Zhou, Cold Reg. Sci. Technol. 103 (2014) 74-81.
22. Y. Zhao, C.L. Wang, L. Ning, H.F. Zhao, and J. Bi, Fuel. 309 (2022) 122112.
23. W.B. Han, G. Zhou, D.H. Gao, Z.X. Zhang, Z.Y. Wei, H.T. Wang, and H.Q. Yang, Powder Technol. 362 (2020) 386-398.
24. H. Rifai, A. Staude, D. Meinel, B. Illerhanus, and G. Bruno, Cem. Concr. Res. 111 (2017) 72-80.
25. D. Ectors, F. Coetz-Neunhoeffer, W.D. Herdeth, U. Dietrich, and J. Neubauer, Cem. Concr. Res. 79 (2016) 366-372.
26. J.J. Chang, W. Yeih, T.J. Chung, and R. Huang, Constr. Build. Mater. 109 (2016) 34-40.
27. M. Rostami and K. Behfarnia, Constr. Build. Mater. 134 (2017) 262-268.
28. K.D. Weerdt, M.B. Haha, G.L. Saout, K.O. Kjellsen, H. Justnes, and B. Lothenbach, Cem. Concr. Res. 41[3] (2011) 279-291.
29. G.D. Moon, S. Oh, S.H. Jung, and Y.C. Choi, Constr. Build. Mater. 135 (2017) 129-136.
30. Q. Wang, J. Yang, and H.H. Chen, Mater and Struct. 50 (2017) 168.
31. A.M. Ramezanianpour and R.D. Hooton, Cem. Concr. Compos. 51 (2014) 1-13.
32. M. Cyr, P. Lawrence, and E. Ringot, Cem. Concr. Res.

36[2] (2006) 264-277.
33. H. Zhang, X. Liu, P. Feng, and W. Wang, Thermochim Acta. 681 (2019) 178403.
34. B.S. Gebregziabiher, R. Thomas, and S. Peethamparan, Cem. Concr. Compos. 55 (2014) 91-102.
35. T. Zhang, B.G. Ma, H.B. Tan, X.H. Liu, P. Chen, and Z.T. Luo, J. Environ. Manage. 276 (2020) 111274.
36. K.L. Scrivener, P. Juilland, and P.J.M. Monteiro, Cem. Concr. Res. 78 (2015) 38-56.
37. Y. He, C.Y. You, M.J. Jiang, S.H. Liu, J.N. Shen, and R.D. Hooton, J. Therm. Anal. Calorim. 148 (2023) 11653-11668.